A Benchmark of Electrostatic Method Performance in Relative Binding Free Energy Calculations

Yunhui Ge,[†] David F. Hahn,[‡] and David L. Mobley[*,¶]

†*Department of Pharmaceutical Sciences, University of California, Irvine, CA 92697, USA*

‡*Computational Chemistry, Janssen Research & Development, Turnhoutseweg 30, Beerse B-2340, Belgium*

¶*Departments of Pharmaceutical Sciences and Chemistry, University of California, Irvine, CA 92697, USA*

E-mail: dmobley@mobleylab.org

ABSTRACT

Relative free energy calculations are fast becoming a critical part of early stage pharmaceutical design, making it important to know how to obtain the best performance with these calculations in applications which could span hundreds of calculations and molecules. In this work, we compared two different treatments of long-range electrostatics, Particle Mesh Ewald (PME) and Reaction Field (RF), in relative binding free energy calculations using a non-equilibrium switching protocol. We found simulations using RF achieve comparable results as those using PME but gain more efficiency when using CPU and similar performance using GPU. The results from this work encourage more use of RF in molecular simulations.

INTRODUCTION

The lead optimization stage is an important part of pharmaceutical drug discovery, involving optimization of several key chemical and biophysical properties in order to ensure candidate compounds have adequate selective binding to their target while also having appropriate other properties to potentially become a new pharmaceutical. Lead optimization efforts always require adequate ligand binding affinity for the target, making this a critical design criterion, and one which is a target for predictive methods. Alchemical relative binding free energy (RBFE) calculations based on molecular dynamics (MD) simulations and statistical mechanics have shown promise in providing reliable predictions to guide experimental work in the context of real drug discovery projects.[1–3]

RBFE calculations compare the potency of two structurally related ligands by transforming one ligand into another via an unphysical or alchemical pathway. This transformation is performed in both the protein-ligand complex and in the solution state to form a closed thermodynamic cycle. The RBFE of the ligands simulated can be calculated through two opposite legs in this cycle.[4,5]

To calculate free energies, these alchemical transformations can be performed via either an equilibrium or non-equilibrium protocol. In general, a number of intermediate simulations are conducted along an alchemical path between the two physical end states, with these simulations being either equilibrium or nonequilibrium depending on the approach chosen. While the free energy difference of interest depends only on the physical end states in the limit of adequate sampling, these intermediate states serve to help obtain converged results and provide sampling which is hopefully adequate. Equilibrium free energy calculations run an equilibrium simulation at each intermediate state as well as the end states which are physically meaningful. In contrast, the non-equilibrium protocol simulates the end states at equilibrium, potentially spending considerably more time there, and only runs short simulations to switch between end states. However, running a large number of switching trials is critical in this case. It is still under debate which of the two protocols is more efficient,

with different studies drawing different conclusions,[6–9] and the choice of protocol is beyond the scope of this paper. This work follows the protocol deployed in a previous work[10] in which a non-equilibrium approach was used, though our results may generalize to equilibrium approaches as well.

Generally, modern MD engines (e.g., AMBER, GROMACS, CHARMM, etc) support different approaches for simulations, including RBFE calculations. Among these software packages, GROMACS is an open source package which is widely used for molecular simulations and reproduces calculated free energies within about 0.2 kcal/mol.[11] Moreover, tools (e.g., pmx[12,13]) allow easy high-throughput applications of GROMACS RBFE simulations, providing a workflow spanning from initial coordinate files to final free energy estimates. This leads to relatively user-friendly RBFE calculations using GROMACS.

Long-range electrostatics interactions are critical in modeling molecular motions in simulations. Due to the computational complexity of such long-range interactions, it becomes challenging to design accurate and efficient methods to describe such interactions. An excellent review of methods for computing the long-range electrostatics interactions in biomolecular simulations can be found here.[14]

Among a number of existing methods, Particle Mesh Ewald (PME)[15,16] is perhaps the most broadly used. PME and other Particle-Mesh methods (e.g., particle-particle particle-mesh method (P3M)[17,18]) are based on the Ewald approach which is a classic method to exactly calculate the electrostatic potential[19] and is chosen as a starting point for further adjustments for better efficiency. In particle-mesh (PM) methods (e.g., PME, P3M) the interaction potential is split into a short-range term (direct sum) and a long-range term (reciprocal sum). The direct part converges fast using a fixed cutoff, and the efficiency of the method is determined by the reciprocal part. The original PME and the smoothed version, smooth PME (which is the implementation of PME method in GROMACS), assign the charges to a grid using Lagrangian interpolation and cardinal B-spline interpolation, respectively. The reciprocal energy and forces can be obtained efficiently using fast Fourier

transforms (FFT). Historically, the PME methods were inspired by the P3M method and later it is shown that they can be mathematically transformed into each other.[20] The algorithms details along with the similarities and differences of the two methods are reviewed by previous work.[17,21–25] It is also somewhat controversial in the literature as to whether P3M and PME should be considered completely equivalent (and share the same name, e.g. P3M); here, however, we do not enter this debate and simply refer to the approach as PME, as this is how the implementation we use is described in the GROMACS documentation.

The PME method finds a balance between the accuracy and efficiency and is widely used in molecular simulations. Additionally, a number of other approaches to long-range electrostatics use similar adaptations of Ewald-based techniques.[17,18,26,27]

While widely used in explicit solvent simulations, Ewald based approaches including PME may also introduce periodicity-induced artifacts which overstabilize the native structure of inherently non-periodic systems. Such artifacts have been extensively explored in previous work and the conclusions are sometimes contradictory suggesting such artifacts are dependent on the system and simulation conditions.[28–37]

Another popular option to compute electrostatics interactions is Reaction Field (RF).[38–40] The RF method only computes the interactions up to a cutoff distance and implicitly treats any interactions beyond the cutoff in a mean-field manner using an appropriate dielectric constant. In this way, electrostatics interactions can be calculated efficiently while hopefully maintaining enough accuracy. However for relatively inhomogeneous systems (e.g., membranes), using RF may introduce artifacts and lead to incorrect modeling of the system. For example, lattice sum electrostatics can be used to represent effectively infinite membranes when simulating membrane proteins, but RF requires a continuum treatment of long-range interactions. Still, RF sees considerable use in the field and can be appealing for suitable system geometries.[41–47]

In this work, we compare the performance of PME and RF methods in RBFE calculations. There is extensive literature comparing RF and Particle-Mesh methods (e.g., PME, P3M) in

plain MD simulations on different systems (e.g., liquids, proteins, etc)[37,40,48–74] which is well summarized in the work of Reif and Oostenbrink.[65] Our focus in this work is specifically on whether these methods yield equivalent relative binding free energies, given the tremendous industrial interest in such calculations. While both RF and PME methods are widely used in free energy calculations,[41–47,75–92] they have not yet been compared head-to-head to see if they yield equivalent results in RBFE calculations, to our knowledge.

METHODS

Selected targets. We selected the targets TYK2[93] and CDK2[94] which are part of several RBFE benchmark studies[2,95,96] including the set commonly referred to as Schrödinger's "JACS set"[95] from a key paper in JACS on large-scale free energy calculations. Among all 8 target systems in the JACS set, TYK2 has a moderate system size ($\sim$ 60000 atoms including water and ions) which yields representative results in performance. CDK2 is the largest system ($\sim$ 110000 atoms including water and ions) among these targets and we selected it to verify the trends observed in TYK2 simulations. For TYK2, we used all 24 edges in our calculations and randomly selected 6 edges of CDK2. The ligands simulated in this work are neutral so no net charge change is involved in each perturbation. A table of successfully simulated perturbations can be found in Table S1, S2.

Molecular Dynamics Simulations. The simulations were performed using GROMACS (2021-dev-20200320-89f1227-unknown) with a patch optimizing PME performance on GPU (`https://gerrit.gromacs.org/c/gromacs/+/13382`).

For each perturbation, two sets of simulations were prepared: solvated ligands and ligand-protein complexes. The initial ligand and protein structures were obtained from a previous published work.[10]

The ligand was parameterized using Open Force Field version 1.0.0 (codenamed "Parsley").[97] Hybrid structures and topologies for the ligand pairs were generated using pmx[12,13]

following a single topology approach. The workflow established a mapping between atoms of two ligands based on the maximum common substructure and conformational alignment while minimizing perturbation and stabilizing the system.

The AMBER ff99sb*ILDN force field[98–100] was used for protein parameterization. Dodecahedral boxes were filled with TIP3P explicit solvent model solvated ligand pairs/ligand-protein complexes and counterions (150 mM NaCl).

For each perturbation, two states were prepared for both in-solution/bound state ligands: state A and state B, representing ligand 1 and ligand 2, respectively. An energy minimization was first performed, followed by a 10 ps NVT equilibration at 298K. Then the production equilibrium simulation (in the NPT ensemble) was performed for 6 ns at 298 K and a pressure of 1 bar. 80 snapshots were extracted from the production simulation. For each snapshot, a non-equilibrium transformation from state A to B (and vice versa) was performed during 50 ps. For each perturbation, 3 replicas of the series of simulations described above were performed leading to a total of 60 ns simulation data to calculate the free energy differences for the ligands in their in-solution/bound states.

The stochastic dynamics thermostat was used to control the temperature in the simulations. The Parrinello-Rahman barostat[101] was applied to keep the pressure constant. All bond lengths were constrained using the LINCS algorithm.[102] The van der Waals interactions were smoothly switched off between 1.0 and 1.1 nm. A dispersion correction for energy and pressure was used. The non-bonded interactions for the alchemical transitions were treated with a modified soft-core potential.[103]

Two different methods implemented in GROMACS were used to treat long-range electrostatic interactions: Particle Mesh Ewald (PME) and Reaction Field (RF). For simulations using PME, a direct space cutoff of 1.1 nm and a Fourier grid spacing of 0.12 nm were used. For simulations using RF, a dielectric constant (ϵ_{rf}) of 78.3, the dielectric constant of water at 298 K was used.[104]

Both CPU and GPU simulations were performed using PME or RF electrostatics. In the

rest of the paper, we denote CPU-PME, CPU-RF, GPU-PME and GPU-RF to represent the hardware and methods for long-range electrostatic interactions treatment.

RESULTS

Predicted relative binding free energies from simulations using RF show good agreement with those from PME. The relative binding free energies ($\Delta\Delta G$) were calculated for a set of modifications of TYK2 (24 $\Delta\Delta G$ values in total) which is also included in a standard test set for relative free energy calculations (the set commonly referred to as Schrödinger's "JACS set" [95] from a key paper in JACS on large-scale free energy calculations). Figure 1 summarizes the computed values using RF/PME on CPU/GPU. The uncertainty estimates were performed by 1000 bootstrapping trials and are reported in Figure 1 as $x_{x_{low}}^{x_{high}}$ where x is the mean value, x_{high} and x_{low} indicate 95% confidence intervals. The averaged root-mean-square error (RMSE) and mean unsigned error (MUE) of $\Delta\Delta G$ for CPU-PME versus CPU-RF are 0.45 and 0.34 kcal/mol and for GPU-PME versus GPU-RF are 0.52, 0.40 kcal/mol, respectively (Figure 1a-b). A cross-platform (CPU vs GPU) comparison also shows essentially the same level of agreement between results using RF and PME (Figure 1c-d) suggesting the same trend holds true on both CPU and GPU.

In this work, we are focused on the comparison between RF and PME methods on relative binding free energy calculations. While comparing calculated $\Delta\Delta G$ with experimental measured values is more important to benchmarking force fields/methodologies, it is not the top interest in this work. However, we summarize our calculated values and the corresponding experimental results in Table S3. In conclusion, the calculated values of both methods are similarly accurate when compared to the experimental values.

Simulations using RF are more efficient than using PME. Given that PME and RF achieve a good level of agreement of calculated $\Delta\Delta G$ values, our focus shifts to computational efficiency, where RF is generally less computationally demanding than using PME [79,105] when

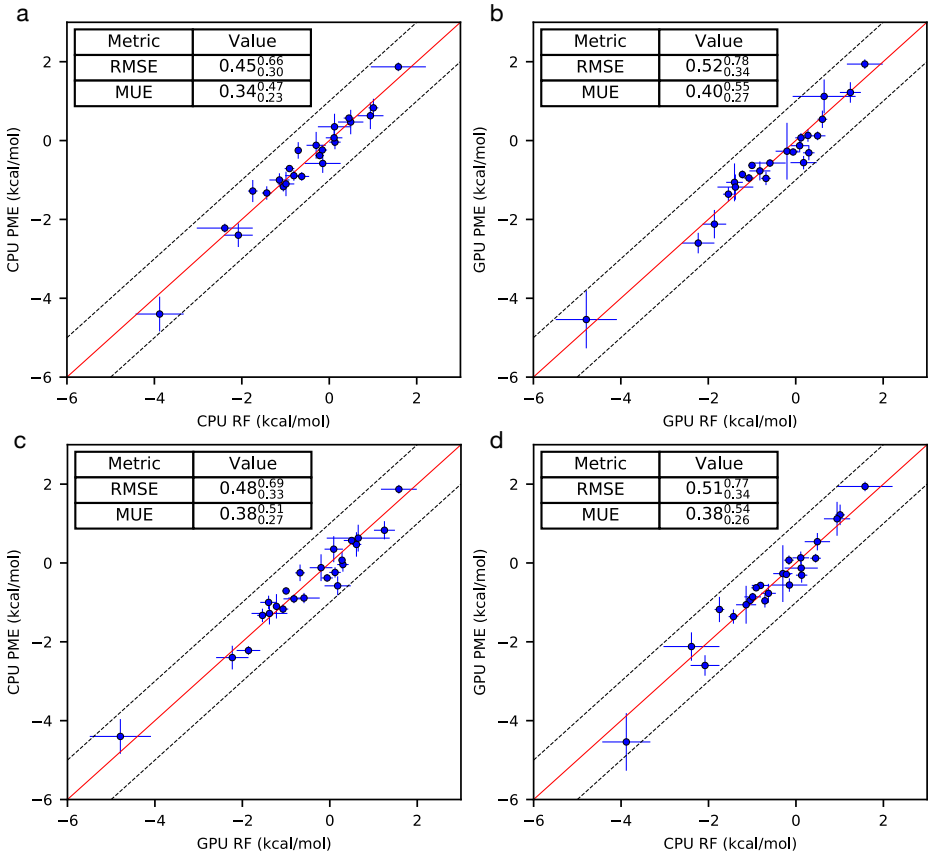

Figure 1: Calculated $\Delta\Delta G$ values of TYK2 ligands using RF/PME on CPU/GPU. Overall, a good agreement is achieved between using PME and RF on CPU/GPU. The uncertainty estimates are calculated by bootstrapping, using 100 bootstrap samples.

the same cut-off is used since more computational time is needed for PME in reciprocal space and tabulated interactions. The simulation performance (in the unit of ns/day) was analyzed from the 6-ns equilibrium NPT simulation and is summarized in Figure 2 where different colors represent using RF/PME on CPU/GPU. The uncertainties were estimated using the standard deviations across different edges. As mentioned in Methods, the simulations were performed in-solution and ligand-bound state in which 5908 $\pm$ 221 atoms and 62290 $\pm$ 6 atoms were simulated, respectively. For the (less costly) in-solution ligand simulations, using RF on CPU is $\sim$30% faster than using PME on average (Figure 2a) and is similar to PME when simulated on GPU considering the uncertainties (Figure 2b). For the more costly bound state simulation, a similar trend is observed in CPU simulations (Figure 2c).

However, using RF on GPU is ∼10% slower than using PME on average (Figure 2d).

The results from Figure 2 show that using RF is faster than PME in most cases for the different system sizes and hardware tested here. It is notable that the GROMACS version used in these simulations was specifically optimized for PME performance on GPU (`https://gerrit.gromacs.org/c/gromacs/+/13382`). Thus, it is not surprising that PME outperformed RF on GPUs (slightly) in our tests here. However, the difference between PME and RF on GPU performance is only minor (∼10%). Possibly a similar optimization of GROMACS for RF on GPUs could yield substantial performance gains.

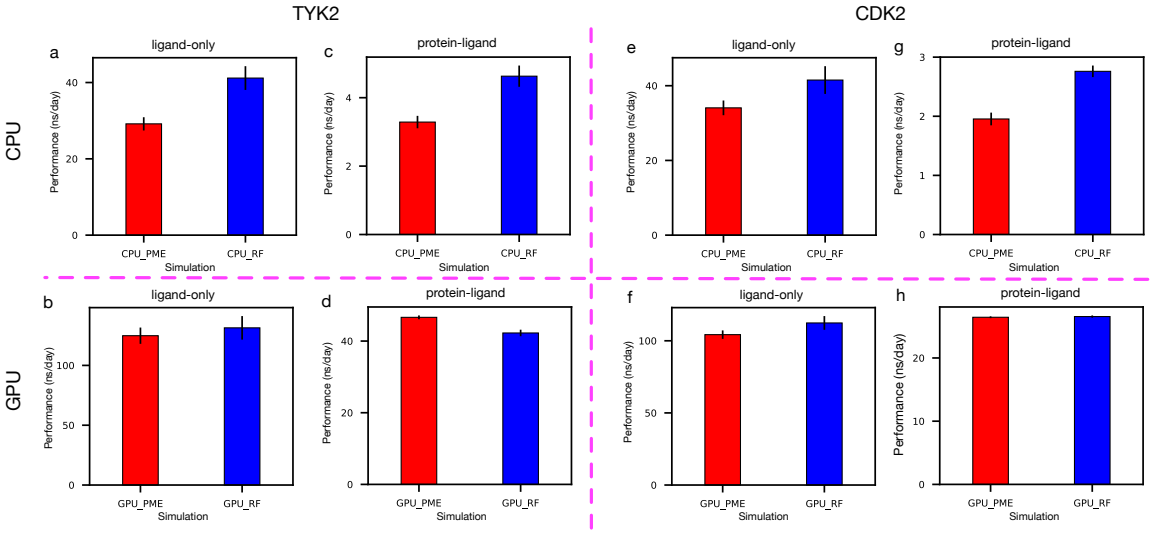

Figure 2: Performance difference between using RF/PME on CPU/GPU in TYK2 simulations of (a-b) ligand-only in-solution, (c-d) protein-ligand complex and in CDK2 simulations of (e-f) ligand-only in-solution, (g-h) protein-ligand complex.

To verify the observed trends in TYK2 simulations, 6 selected edges from CDK2 were simulated using the same protocol described in METHOD. CDK2 is a larger system than TYK2 and has 5602 ± 373 and 106908 ± 5 atoms in in-solution and ligand-bound state simulation, respectively. Similar to the results of TYK2, simulations using RF are also faster (∼20-40%) than using PME on CPU (Figure 2e,g). Notably, GPU simulations using RF achieves a similar efficiency to PME (Figure 2f,h) which means even with optimizations, PME still cannot surpass RF in efficiency (Figure 2d).

Figure 2 shows that using RF is more efficient than PME on CPUs and is comparable to PME in GPU simulations. This is remarkable given the fact the GROMACS used in this work is optimized for PME performance on GPU. RF could perhaps become even more promising with further optimizations.

On average, the protein-ligand complex simulation of each TYK2 perturbation took 31.7 hours using RF and 47.3 hours using PME on 8 CPUs ($\sim$ 30% performance gain using RF), with the protocol used here. With same setup, the ligand-only simulation of TYK2 took 3.5 and 4.8 hours using RF and PME, respectively (also $\sim$ 30% performance gain using RF). When using 1 GPU, a calculation time of 3.4 hours using RF and 3.1 hours using PME was needed for protein-ligand complex simulations ($\sim$ 10% performance gain using PME). In ligand-only simulation on 1 GPU, an average time of 1.1 and 1.2 hours was needed using RF and PME, respectively ($\sim$ 10% performance gain using RF). A summary of simulation wallclock time can be found in Table S4 and S5.

Here, while we find that PME and RF achieve comparable results within uncertainty, this is with present-day force fields, and may not always be the case in future studies. It is not too difficult to imagine a scenario where force fields might be optimized for the best performance with a particular model of long range electrostatics, such as a force field designed for use with PME, or one for use with RF. Once force fields are tuned for specific electrostatics treatments, it is reasonable to expect that results might differ in quality if the electrostatics treatment is changed. To some extent, we already see such tuning taking place for water models (e.g. the SPC/E, TIP4P-Ew, and TIP5P-E models designed for use with Ewald-based electrostatics[106–110]), though not yet for other components of the force field to our knowledge. Still, results from these water studies indicate that electrostatics treatment, or at least the switch from cutoff based to lattice-sum electrostatics, impacts bulk properties enough that the choice of electrostatics treatment should perhaps be considered part of the force field. So, perhaps future force fields should require a particular choice of long range electrostatics treatment, and separate Ewald-based and RF-based versions should be fitted.

CONCLUSION

The treatment of long-range electrostatic interactions is critical for a correct modeling of (bio)molecular systems in molecular dynamics simulations. Due to the long-range nature and N^2-scaling of electrostatic interactions, they are computationally the most demanding terms in the force field evaluation. Both PME and RF are popular methods of treating long range electrostatic interactions. PME is widely used and attempts to find a good balance between efficiency and accuracy, but we find that RF achieves higher efficiency, although it may have some limitations in relatively inhomogeneous systems such as for membrane simulations.

We expect the results observed in this work will be generalizable to other simulation packages and force fields, in that results will not be highly dependent on PME vs RF, but (a) that is outside of scope for this work, and (b) details will depend on the exact implementation in those software packages. Previous work has shown that different simulation engines are able to take in the same force field and same systems and give identical energies (with PME) within a reasonable tolerance, which would strongly suggest the implementations are equivalent or nearly so,[111,112] at least for PME.

The conclusions presented in this work are true only for neutral perturbations and are not guaranteed in other perturbations (e.g., charge-changing mutations). When charged species are involved, different correction schemes must be applied to correct the bias induced by electrostatics finite-size effects depending on electrostatic treatment methods used (e.g., RF, PME).[113–118]

This work is focused on comparing the results and performance of PME and RF for relative binding free energy calculations. We found the calculated $\Delta\Delta G$ values are in good agreement using PME and RF whereas simulations using RF are comparable or faster than PME on both CPU and GPU. Taken the results presented here, we suggest that RF may be a promising option for relative free energy simulations because , at least in GROMACS, it is less computationally demanding while retaining comparable accuracy to PME. This advantage

may be particularly helpful in cases where a large number of simulations are needed (e.g., in the lead optimization stage of the drug discovery process). Thus we recommend free energy calculations with RF be considered as a viable option, at least for homogeneous systems.

ACKNOWLEDGEMENTS

DLM appreciates financial support from the National Institutes of Health (R01GM108889 and R01GM132386). We appreciate the Open Force Field Consortium for its support of the Open Force Field Initiative, which provided software infrastructure used in this work.

Supporting Information Available

Supporting information (simulated system size, calculated/experimental relative binding free energies, simulation wallclock time) is available free of charge via the Internet at `http://pubs.acs.org`.

Data and Software Availability

Datasets. All input files for simulations, data and scripts for analysis are freely available at `https://github.com/MobleyLab/PME-RF-benchmark`.

Software. Simulations were performed using the open-source molecular dynamics package GROMACS with a specific patch optimizing PME performance on GPUs. Analysis was performed using pmx and PLBenchmarks. The versions of both packages used in this work are freely distributed at `https://github.com/MobleyLab/PME-RF-benchmark/tree/main/SI/analysis` with installation instructions.

Notes

D.L.M. is a member of the Scientific Advisory Board of OpenEye Scientific Software and an Open Science Fellow with Silicon Therapeutics.

References

(1) Cournia, Z.; Allen, B.; Sherman, W. Relative Binding Free Energy Calculations in Drug Discovery: Recent Advances and Practical Considerations. *J. Chem. Inf. Model.* **2017**, *57*, 2911–2937.

(2) Song, L. F.; Lee, T.-S.; Zhu, C.; York, D. M.; Merz, K. M. Using AMBER18 for Relative Free Energy Calculations. *J. Chem. Inf. Model.* **2019**, *59*, 3128–3135.

(3) Schindler, C. E. M.; Baumann, H.; Blum, A.; Böse, D.; Buchstaller, H.-P.; Burgdorf, L.; Cappel, D.; Chekler, E.; Czodrowski, P.; Dorsch, D.; Eguida, M. K. I.; Follows, B.; Fuchß, T.; Grädler, U.; Gunera, J.; Johnson, T.; Jorand Lebrun, C.; Karra, S.; Klein, M.; Knehans, T.; Koetzner, L.; Krier, M.; Leiendecker, M.; Leuthner, B.; Li, L.; Mochalkin, I.; Musil, D.; Neagu, C.; Rippmann, F.; Schiemann, K.; Schulz, R.; Steinbrecher, T.; Tanzer, E.-M.; Unzue Lopez, A.; Viacava Follis, A.; Wegener, A.; Kuhn, D. Large-Scale Assessment of Binding Free Energy Calculations in Active Drug Discovery Projects. *J. Chem. Inf. Model.* **2020**, *60*, 5457–5474.

(4) Tembre, B. L.; Mc Cammon, J. Ligand-receptor interactions. *Comput. Chem. (Oxford, U. K.)* **1984**, *8*, 281 – 283.

(5) Mey, A. S. J. S.; Allen, B. K.; Macdonald, H. E. B.; Chodera, J. D.; Hahn, D. F.; Kuhn, M.; Michel, J.; Mobley, D. L.; Naden, L. N.; Prasad, S.; Rizzi, A.; Scheen, J.; Shirts, M. R.; Tresadern, G.; Xu, H. Best Practices for Alchemical Free Energy Calculations [Article v1.0]. *LiveCoMS* **2020**, *2*, 18378.

(6) Ytreberg, F. M.; Swendsen, R. H.; Zuckerman, D. M. Comparison of Free Energy Methods for Molecular Systems. *J. Chem. Phys.* **2006**, *125*, 184114.

(7) Goette, M.; Grubmüller, H. Accuracy and Convergence of Free Energy Differences Calculated from Nonequilibrium Switching Processes. *J. Comput. Chem.* **2009**, *30*, 447–456.

(8) Yildirim, A.; Wassenaar, T. A.; van der Spoel, D. Statistical Efficiency of Methods for Computing Free Energy of Hydration. *J. Chem. Phys.* **2018**, *149*, 144111.

(9) Baumann, H.; Gapsys, V.; de Groot, B. L.; Mobley, D. Challenges Encountered Applying Equilibrium and Non-Equilibrium Binding Free Energy Calculations. *ChemRxiv* **2020**,

(10) Gapsys, V.; Pérez-Benito, L.; Aldeghi, M.; Seeliger, D.; van Vlijmen, H.; Tresadern, G.; de Groot, B. L. Large Scale Relative Protein Ligand Binding Affinities Using Non-Equilibrium Alchemy. *Chem. Sci.* **2020**, *11*, 1140–1152.

(11) Loeffler, H. H.; Bosisio, S.; Duarte Ramos Matos, G.; Suh, D.; Roux, B.; Mobley, D. L.; Michel, J. Reproducibility of Free Energy Calculations across Different Molecular Simulation Software Packages. *J. Chem. Theory Comput.* **2018**, *14*, 5567–5582.

(12) Seeliger, D.; de Groot, B. L. Protein Thermostability Calculations Using Alchemical Free Energy Simulations. *Biophys. J.* **2010**, *98*, 2309–2316.

(13) Gapsys, V.; Michielssens, S.; Seeliger, D.; de Groot, B. L. Pmx: Automated Protein Structure and Topology Generation for Alchemical Perturbations. *J. Comput. Chem.* **2015**, *36*, 348–354.

(14) Cisneros, G. A.; Karttunen, M.; Ren, P.; Sagui, C. Classical Electrostatics for Biomolecular Simulations. *Chem. Rev.* **2014**, *114*, 779–814.

(15) Darden, T.; York, D.; Pedersen, L. Particle mesh Ewald: An N·log(N) method for Ewald sums in large systems. *J. Chem. Phys.* **1993**, *98*, 10089–10092.

(16) Essmann, U.; Perera, L.; Berkowitz, M. L.; Darden, T.; Lee, H.; Pedersen, L. G. A smooth particle mesh Ewald method. *J. Chem. Phys.* **1995**, *103*, 8577–8593.

(17) Pollock, E. L.; Glosli, J. Comments on P3M, FMM, and the Ewald method for large periodic Coulombic systems. *Comput. Phys. Commun.* **1996**, *95*, 93–110.

(18) Hockney, R. W.; Eastwood, J. W. *Computer Simulation Using Particles*; McGraw-Hill: New York, 1981.

(19) Ewald, P. P. Die Berechnung optischer und elektrostatischer Gitterpotentiale. *Ann. Phys.* **1921**, *369*, 253–287.

(20) Ballenegger, V.; Cerdà, J. J.; Holm, C. How to Convert SPME to P3M: Influence Functions and Error Estimates. *J. Chem. Theory Comput.* **2012**, *8*, 936–947.

(21) Wang, H.; Dommert, F.; Holm, C. Optimizing working parameters of the smooth particle mesh Ewald algorithm in terms of accuracy and efficiency. *J. Chem. Phys.* **2010**, *133*, 034117–13.

(22) Ballenegger, V.; Cerdà, J. J.; Lenz, O.; Holm, C. The optimal P3M algorithm for computing electrostatic energies in periodic systems. *J. Chem. Phys.* **2008**, *128*, 034109–14.

(23) Deserno, M.; Holm, C. How to mesh up Ewald sums. I. A theoretical and numerical comparison of various particle mesh routines. *J. Chem. Phys.* **1998**, *109*, 7678–7693.

(24) Sagui, C.; Darden, T. A. Molecular Dynamics Simulations of Biomolecules: Long-Range Electrostatic Effects. *Annu. Rev. Biophys. Biomol. Struct.* **1999**, *28*, 155–179.

(25) Sagui, C.; Darden, T. A. P3M and PME: A comparison of the two methods. *AIP Conf. Proc.* **1999**, *492*, 104–113.

(26) York, D.; Yang, W. The fast Fourier Poisson method for calculating Ewald sums. *J. Chem. Phys.* **1994**, *101*, 3298–3300.

(27) Sagui, C.; Darden, T. Multigrid methods for classical molecular dynamics simulations of biomolecules. *J. Chem. Phys.* **2001**, *114*, 6578–6591.

(28) Auffinger, P.; Louise-May, S.; Westhof, E. Molecular Dynamics Simulations of the Anticodon Hairpin of $tRNA^{Asp}$: Structuring Effects of C-H$\cdots$O Hydrogen Bonds and of Long-Range Hydration Forces. *J. Am. Chem. Soc.* **1996**, *118*, 1181–1189.

(29) Hunenberger, P. H.; McCammon, J. A. Effect of artificial periodicity in simulations of biomolecules under Ewald boundary conditions: a continuum electrostatics study. *Biophys. Chem.* **1999**, *78*, 69–88.

(30) Kastenholz, M. A.; Hünenberger, P. H. Influence of Artificial Periodicity and Ionic Strength in Molecular Dynamics Simulations of Charged Biomolecules Employing Lattice-Sum Methods. *J. Phys. Chem. B* **2004**, *108*, 774–788.

(31) Smith, P. E.; Blatt, H. D.; Pettitt, B. M. On the Presence of Rotational Ewald Artifacts in the Equilibrium and Dynamical Properties of a Zwitterionic Tetrapeptide in Aqueous Solution. *J. Phys. Chem. B* **1997**, *101*, 3886–3890.

(32) Weber, W.; Hünenberger, P. H.; McCammon, J. A. Molecular Dynamics Simulations of a Polyalanine Octapeptide under Ewald Boundary Conditions: Influence of Artificial Periodicity on Peptide Conformation. *J. Phys. Chem. B* **2000**, *104*, 3668–3675.

(33) Kastenholz, M. A.; Hünenberger, P. H. Development of a lattice-sum method emulating nonperiodic boundary conditions for the treatment of electrostatic interactions in molecular simulations: A continuum-electrostatics study. *J. Chem. Phys.* **2006**, *124*, 124108–13.

(34) Wu, X.; Brooks, B. R. Isotropic periodic sum: A method for the calculation of long-range interactions. *J. Chem. Phys.* **2005**, *122*, 044107–19.

(35) Smith, P. E.; Pettitt, B. M. Ewald artifacts in liquid state molecular dynamics simulations. *J. Chem. Phys.* **1996**, *105*, 4289–4293.

(36) Fox, T.; Kollman, P. A. The application of different solvation and electrostatic models in molecular dynamics simulations of ubiquitin: How well is the X-ray structure "maintained"? *Proteins: Struct., Funct., Bioinf.* **1996**, *25*, 315–334.

(37) de Vries, A. H.; Chandrasekhar, I.; van Gunsteren, W. F.; Hünenberger, P. H. Molecular Dynamics Simulations of Phospholipid Bilayers: Influence of Artificial Periodicity, System Size, and Simulation Time. *J. Phys. Chem. B* **2005**, *109*, 11643–11652.

(38) Barker, J. A.; Watts, R. O. Monte Carlo studies of the dielectric properties of water-like models. *Mol. Phys.* **1973**, *26*, 789–792.

(39) Barker, J. A. Reaction field, screening, and long-range interactions in simulations of ionic and dipolar systems. *Mol. Phys.* **1994**, *83*, 1057–1064.

(40) Tironi, I. G.; Sperb, R.; Smith, P. E.; van Gunsteren, W. F. A generalized reaction field method for molecular dynamics simulations. *J. Chem. Phys.* **1995**, *102*, 5451–5459.

(41) Stjernschantz, E.; Oostenbrink, C. Improved Ligand-Protein Binding Affinity Predictions Using Multiple Binding Modes. *Biophys. J.* **2010**, *98*, 2682–2691.

(42) Lai, B.; Oostenbrink, C. Binding free energy, energy and entropy calculations using simple model systems. *Theor. Chem. Acc.* **2012**, *131*, 23–13.

(43) Dolenc, J.; Oostenbrink, C.; Koller, J.; van Gunsteren, W. F. Molecular dynamics simulations and free energy calculations of netropsin and distamycin binding to an AAAAA DNA binding site. *Nucleic Acids Res.* **2005**, *33*, 725–733.

(44) Perthold, J. W.; Oostenbrink, C. Simulation of Reversible Protein–Protein Binding and Calculation of Binding Free Energies Using Perturbed Distance Restraints. *J. Chem. Theory Comput.* **2017**, *13*, 5697–5708.

(45) Oostenbrink, C.; van Gunsteren, W. F. Free energies of binding of polychlorinated biphenyls to the estrogen receptor from a single simulation. *Proteins: Struct., Funct., Bioinf.* **2004**, *54*, 237–246.

(46) Bren, U.; Oostenbrink, C. Cytochrome P450 3A4 Inhibition by Ketoconazole: Tackling the Problem of Ligand Cooperativity Using Molecular Dynamics Simulations and Free-Energy Calculations. *J. Chem. Inf. Model.* **2012**, *52*, 1573–1582.

(47) de Ruiter, A.; Boresch, S.; Oostenbrink, C. Comparison of thermodynamic integration and Bennett acceptance ratio for calculating relative protein-ligand binding free energies. *J. Comput. Chem.* **2013**, *34*, 1024–1034.

(48) Neumann, M.; Steinhauser, O.; Stuart Pawley, G. Consistent calculation of the static and frequency-dependent dielectric constant in computer simulations. *Mol. Phys.* **1984**, *52*, 97–113.

(49) Belhadj, M.; Alper, H. E.; Levy, R. M. Molecular-Dynamics Simulations of Water with Ewald Summation for the Long-Range Electrostatic Interactions. *Chem. Phys. Lett.* **1991**, *179*, 13–20.

(50) Perera, L.; Essmann, U.; Berkowitz, M. L. Effect of the treatment of long-range forces on the dynamics of ions in aqueous solutions. *J. Chem. Phys.* **1995**, *102*, 450–456.

(51) Hummer, G.; Soumpasis, D. M.; Neumann, M. Pair correlations in an NaCl-SPC water model. *Mol. Phys.* **1992**, *77*, 769–785.

(52) Tironi, I. G.; Luty, B. A.; van Gunsteren, W. F. Space-time correlated reaction field:

A stochastic dynamical approach to the dielectric continuum. *J. Chem. Phys.* **1997**, *106*, 6068–6075.

(53) Hünenberger, P. H.; van Gunsteren, W. F. Alternative schemes for the inclusion of a reaction-field correction into molecular dynamics simulations: Influence on the simulated energetic, structural, and dielectric properties of liquid water. *J. Chem. Phys.* **1998**, *108*, 6117–6134.

(54) Nymand, T. M.; Linse, P. Molecular dynamics simulations of polarizable water at different boundary conditions. *J. Chem. Phys.* **2000**, *112*, 6386–6395.

(55) Arbuckle, B. W.; Clancy, P. Effects of the Ewald sum on the free energy of the extended simple point charge model for water. *J. Chem. Phys.* **2002**, *116*, 5090–10.

(56) Mathias, G.; Egwolf, B.; Nonella, M.; Tavan, P. A fast multipole method combined with a reaction field for long-range electrostatics in molecular dynamics simulations: The effects of truncation on the properties of water. *J. Chem. Phys.* **2003**, *118*, 10847–10860.

(57) Hünenberger, P. H.; McCammon, J. A. Ewald artifacts in computer simulations of ionic solvation and ion–ion interaction: A continuum electrostatics study. *J. Chem. Phys.* **1999**, *110*, 1856–1872.

(58) English, N. J. Molecular dynamics simulations of liquid water using various long-range electrostatics techniques. *Mol. Phys.* **2005**, *103*, 1945–1960.

(59) Fennell, C. J.; Gezelter, J. D. Is the Ewald summation still necessary? Pairwise alternatives to the accepted standard for long-range electrostatics. *J. Chem. Phys.* **2006**, *124*, 234104–13.

(60) Boresch, S.; Steinhauser, O. Rationalizing the effects of modified electrostatic inter-

actions in computer simulations: The dielectric self-consistent field method. *J. Chem. Phys.* **1999**, *111*, 8271–8274.

(61) Peter, C.; van Gunsteren, W. F.; Hünenberger, P. H. A fast-Fourier transform method to solve continuum-electrostatics problems with truncated electrostatic interactions: Algorithm and application to ionic solvation and ion–ion interaction. *J. Chem. Phys.* **2003**, *119*, 12205–12223.

(62) Rozanska, X.; Chipot, C. Modeling ion–ion interaction in proteins: A molecular dynamics free energy calculation of the guanidinium-acetate association. *J. Chem. Phys.* **2000**, *112*, 9691–9694.

(63) Baumketner, A.; Shea, J.-E. The Influence of Different Treatments of Electrostatic Interactions on the Thermodynamics of Folding of Peptides †. *J. Phys. Chem. B* **2005**, *109*, 21322–21328.

(64) Lins, R. D.; Röthlisberger, U. Influence of Long-Range Electrostatic Treatments on the Folding of the N-Terminal H4 Histone Tail Peptide. *J. Chem. Theory Comput.* **2006**, *2*, 246–250.

(65) Reif, M. M.; Kräutler, V.; Kastenholz, M. A.; Daura, X.; Hünenberger, P. H. Molecular Dynamics Simulations of a Reversibly Folding β-Heptapeptide in Methanol: Influence of the Treatment of Long-Range Electrostatic Interactions. *J. Phys. Chem. B* **2009**, *113*, 3112–3128.

(66) Walser, R.; Hunenberger, P. H.; van Gunsteren, W. F. Comparison of different schemes to treat long-range electrostatic interactions in molecular dynamics simulations of a protein crystal. *Proteins: Struct., Funct., Bioinf.* **2001**, *43*, 509–519.

(67) Walser, R.; Hünenberger, P. H.; van Gunsteren, W. F. Molecular dynamics simulations of a double unit cell in a protein crystal: Volume relaxation at constant pressure and

correlation of motions between the two unit cells. *Proteins: Struct., Funct., Bioinf.* **2002**, *48*, 327–340.

(68) Gargallo, R.; Hunenberger, P. H.; Aviles, F. X.; Oliva, B. Molecular dynamics simulation of highly charged proteins: Comparison of the particle-particle particle-mesh and reaction field methods for the calculation of electrostatic interactions. *Protein Sci.* **2003**, *12*, 2161–2172.

(69) Nina, M.; Simonson, T. Molecular Dynamics of the tRNA AlaAcceptor Stem: Comparison between Continuum Reaction Field and Particle-Mesh Ewald Electrostatic Treatments. *J. Phys. Chem. B* **2002**, *106*, 3696–3705.

(70) Kräutler, V.; Hünenberger, P. H. Explicit-solvent molecular dynamics simulations of a DNA tetradecanucleotide duplex: lattice-sum versus reaction-field electrostatics. *Mol. Simul.* **2008**, *34*, 491–499.

(71) Tieleman, D. P.; Hess, B.; Sansom, M. S. P. Analysis and Evaluation of Channel Models: Simulations of Alamethicin. *Biophys. J.* **2002**, *83*, 2393–2407.

(72) Anézo, C.; de Vries, A. H.; Höltje, H.-D.; Tieleman, D. P.; Marrink, S.-J. Methodological Issues in Lipid Bilayer Simulations. *J. Phys. Chem. B* **2003**, *107*, 9424–9433.

(73) Patra, M.; Karttunen, M.; Hyvönen, M. T.; Falck, E.; Vattulainen, I. Lipid Bilayers Driven to a Wrong Lane in Molecular Dynamics Simulations by Subtle Changes in Long-Range Electrostatic Interactions. *J. Phys. Chem. B* **2004**, *108*, 4485–4494.

(74) Robertson, A.; Luttmann, E.; Pande, V. S. Effects of long-range electrostatic forces on simulated protein folding kinetics. *J. Comput. Chem.* **2008**, *29*, 694–700.

(75) Kuhn, M.; Firth-Clark, S.; Tosco, P.; Mey, A. S. J. S.; Mackey, M.; Michel, J. Assessment of Binding Affinity via Alchemical Free-Energy Calculations. *J. Chem. Inf. Model.* **2020**, *60*, 3120–3130.

(76) Loeffler, H. H.; Bosisio, S.; Matos, G. D. R.; Suh, D.; Roux, B.; Mobley, D. L.; Michel, J. Reproducibility of Free Energy Calculations across Different Molecular Simulation Software Packages. *J. Chem. Theory Comput.* **2018**, *14*, 5567–5582.

(77) Gapsys, V.; Pérez-Benito, L.; Aldeghi, M.; Seeliger, D.; van Vlijmen, H.; Tresadern, G.; de Groot, B. L. Large scale relative protein ligand binding affinities using non-equilibrium alchemy. *Chem. Sci.* **2020**, *11*, 1140–1152.

(78) Zhou, R.; Das, P.; Royyuru, A. K. Single Mutation Induced H3N2 Hemagglutinin Antibody Neutralization: A Free Energy Perturbation Study. *J. Phys. Chem. B* **2008**, *112*, 15813–15820.

(79) Garrido, N. M.; Jorge, M.; Queimada, A. J.; Economou, I. G.; Macedo, E. A. Molecular simulation of the hydration Gibbs energy of barbiturates. *Fluid Phase Equilib.* **2010**, *289*, 148–155.

(80) Procacci, P.; Guarnieri, G. SAMPL7 blind predictions using nonequilibrium alchemical approaches. *J. Comput.-Aided Mol. Des.* **2021**, *28*, 305–11.

(81) Huai, Z.; Yang, H.; Li, X.; Sun, Z. SAMPL7 TrimerTrip host–guest binding affinities from extensive alchemical and end-point free energy calculations. *J. Comput.-Aided Mol. Des.* **2020**, *44*, 338–13.

(82) Khalak, Y.; Tresadern, G.; de Groot, B. L.; Gapsys, V. Non-equilibrium approach for binding free energies in cyclodextrins in SAMPL7: force fields and software. *J. Comput.-Aided Mol. Des.* **2020**, *26*, 473–13.

(83) Shi, Y.; Laury, M. L.; Wang, Z.; Ponder, J. W. AMOEBA binding free energies for the SAMPL7 TrimerTrip host–guest challenge. *J. Comput.-Aided Mol. Des.* **2020**, *115*, 12320–15.

(84) Manzoni, F.; Söderhjelm, P. Prediction of hydration free energies for the SAMPL4 data set with the AMOEBA polarizable force field. *J. Comput.-Aided Mol. Des.* **2014**, *28*, 235–244.

(85) Yin, J.; Henriksen, N. M.; Slochower, D. R.; Gilson, M. K. The SAMPL5 host–guest challenge: computing binding free energies and enthalpies from explicit solvent simulations by the attach-pull-release (APR) method. *J. Comput.-Aided Mol. Des.* **2016**, *31*, 133–145.

(86) Beckstein, O.; Fourrier, A.; Iorga, B. I. Prediction of hydration free energies for the SAMPL4 diverse set of compounds using molecular dynamics simulations with the OPLS-AA force field. *J. Comput.-Aided Mol. Des.* **2014**, *28*, 265–276.

(87) Mikulskis, P.; Cioloboc, D.; Andrejić, M.; Khare, S.; Brorsson, J.; Genheden, S.; Mata, R. A.; Söderhjelm, P.; Ryde, U. Free-energy perturbation and quantum mechanical study of SAMPL4 octa-acid host–guest binding energies. *J. Comput.-Aided Mol. Des.* **2014**, *28*, 375–400.

(88) Aldeghi, M.; Heifetz, A.; Bodkin, M. J.; Knapp, S.; Biggin, P. C. Accurate calculation of the absolute free energy of binding for drug molecules. *Chem. Sci.* **2016**, *7*, 207–218.

(89) Araujo, S. C.; Maltarollo, V. G.; Almeida, M. O.; Ferreira, L. L. G.; Andricopulo, A. D.; Honorio, K. M. Structure-Based Virtual Screening, Molecular Dynamics and Binding Free Energy Calculations of Hit Candidates as ALK-5 Inhibitors. *Molecules* **2020**, *25*, 264–14.

(90) Woo, H.-J.; Roux, B. Calculation of absolute protein-ligand binding free energy from computer simulations. *Proc. Natl. Acad. Sci. U. S. A.* **2005**, *102*, 6825–6830.

(91) Mobley, D. L.; Graves, A. P.; Chodera, J. D.; McReynolds, A. C.; Shoichet, B. K.; Dill, K. A. Predicting Absolute Ligand Binding Free Energies to a Simple Model Site. *J. Mol. Biol.* **2007**, *371*, 1118–1134.

(92) Shivakumar, D.; Williams, J.; Wu, Y.; Damm, W.; Shelley, J.; Sherman, W. Prediction of Absolute Solvation Free Energies using Molecular Dynamics Free Energy Perturbation and the OPLS Force Field. *J. Chem. Theory Comput.* **2010**, *6*, 1509–1519.

(93) Liang, J.; Tsui, V.; Van Abbema, A.; Bao, L.; Barrett, K.; Beresini, M.; Berezhkovskiy, L.; Blair, W. S.; Chang, C.; Driscoll, J.; Eigenbrot, C.; Ghilardi, N.; Gibbons, P.; Halladay, J.; Johnson, A.; Kohli, P. B.; Lai, Y.; Liimatta, M.; Mantik, P.; Menghrajani, K.; Murray, J.; Sambrone, A.; Xiao, Y.; Shia, S.; Shin, Y.; Smith, J.; Sohn, S.; Stanley, M.; Ultsch, M.; Zhang, B.; Wu, L. C.; Magnuson, S. Lead identification of novel and selective TYK2 inhibitors. *Eur. J. Med. Chem.* **2013**, *67*, 175–187.

(94) Hardcastle, I. R.; Arris, C. E.; Bentley, J.; Boyle, F. T.; Chen, Y.; Curtin, N. J.; Endicott, J. A.; Gibson, A. E.; Golding, B. T.; Griffin, R. J.; Jewsbury, P.; Menyerol, J.; Mesguiche, V.; Newell, D. R.; Noble, M. E. M.; Pratt, D. J.; Wang, L. Z.; Whitfield, H. J. N2-substituted O6-cyclohexylmethylguanine derivatives: Potent inhibitors of cyclin-dependent kinases 1 and 2. *J. Med. Chem.* **2004**, *47*, 3710–3722.

(95) Wang, L.; Wu, Y.; Deng, Y.; Kim, B.; Pierce, L.; Krilov, G.; Lupyan, D.; Robinson, S.; Dahlgren, M. K.; Greenwood, J.; Romero, D. L.; Masse, C.; Knight, J. L.; Steinbrecher, T.; Beuming, T.; Damm, W.; Harder, E.; Sherman, W.; Brewer, M.; Wester, R.; Murcko, M.; Frye, L.; Farid, R.; Lin, T.; Mobley, D. L.; Jorgensen, W. L.; Berne, B. J.; Friesner, R. A.; Abel, R. Accurate and Reliable Prediction of Relative Ligand Binding Potency in Prospective Drug Discovery by Way of a Modern Free-Energy Calculation Protocol and Force Field. *J. Am. Chem. Soc.* **2015**, *137*, 2695–2703.

(96) Kuhn, M.; Firth-Clark, S.; Tosco, P.; Mey, A. S. J. S.; Mackey, M.; Michel, J. Assessment of Binding Affinity via Alchemical Free-Energy Calculations. *J. Chem. Inf. Model.* **2020**, *60*, 3120–3130.

(97) Qiu, Y.; Smith, D. G. A.; Boothroyd, S.; Jang, H.; Wagner, J.; Bannan, C. C.;

Gokey, T.; Lim, V. T.; Stern, C. D.; Rizzi, A.; Lucas, X.; Tjanaka, B.; Shirts, M. R.; Gilson, M. K.; Chodera, J. D.; Bayly, C. I.; Mobley, D. L.; Wang, L.-P. Development and Benchmarking of Open Force Field v1.0.0, the Parsley Small Molecule Force Field. *ChemRxiv* **2020**,

(98) Hornak, V.; Abel, R.; Okur, A.; Strockbine, B.; Roitberg, A.; Simmerling, C. Comparison of Multiple Amber Force Fields and Development of Improved Protein Backbone Parameters. *Proteins: Struct., Funct., Bioinf.* **2006**, *65*, 712–725.

(99) Best, R. B.; Hummer, G. Optimized Molecular Dynamics Force Fields Applied to the Helix-Coil Transition of Polypeptides. *J. Phys. Chem. B* **2009**, *113*, 9004–9015.

(100) Lindorff-Larsen, K.; Piana, S.; Palmo, K.; Maragakis, P.; Klepeis, J. L.; Dror, R. O.; Shaw, D. E. Improved Side-Chain Torsion Potentials for the Amber ff99SB Protein Force Field: Improved Protein Side-Chain Potentials. *Proteins: Struct., Funct., Bioinf.* **2010**, *78*, 1950–1958.

(101) Parrinello, M.; Rahman, A. Polymorphic Transitions in Single Crystals: A New Molecular Dynamics Method. *J. Appl. Phys.* **1981**, *52*, 7182–7190.

(102) Hess, B.; Bekker, H.; Berendsen, H. J. C. LINCS: A Linear Constraint Solver for Molecular Simulations. *J. Comput. Chem.* **1997**, *18*, 1463–1472.

(103) Gapsys, V.; Seeliger, D.; de Groot, B. L. New Soft-Core Potential Function for Molecular Dynamics Based Alchemical Free Energy Calculations. *J. Chem. Theory Comput.* **2012**, *8*, 2373–2382.

(104) Malmberg, C. G.; Maryott, A. A. Dielectric Constant of Water From 0-Degrees-C to 100-Degrees-C. *J. Res. Natl. Bur. Stand. (U. S.)* **1956**, *56*, 1–8.

(105) Monticelli, L.; Simões, C.; Belvisi, L.; Colombo, G. Assessing the influence of elec-

trostatic schemes on molecular dynamics simulations of secondary structure forming peptides. *J. Phys.: Condens. Matter* **2006**, *18*, S329–S345.

(106) Berendsen, H. J. C.; Grigera, J. R.; Straatsma, T. P. The Missing Term in Effective Pair Potentials. *J. Phys. Chem.* **1987**, *91*, 6269–6271.

(107) Chatterjee, S.; Debenedetti, P. G.; Stillinger, F. H.; Lynden-Bell, R. M. A Computational Investigation of Thermodynamics, Structure, Dynamics and Solvation Behavior in Modified Water Models. *J. Chem. Phys.* **2008**, *128*, 124511.

(108) Horn, H. W.; Swope, W. C.; Pitera, J. W.; Madura, J. D.; Dick, T. J.; Hura, G. L.; Head-Gordon, T. Development of an Improved Four-Site Water Model for Biomolecular Simulations: TIP4P-Ew. *J. Chem. Phys.* **2004**, *120*, 9665–9678.

(109) Horn, H. W.; Swope, W. C.; Pitera, J. W. Characterization of the TIP4P-Ew Water Model: Vapor Pressure and Boiling Point. *J. Chem. Phys.* **2005**, *123*, 194504.

(110) Rick, S. W. A Reoptimization of the Five-Site Water Potential (TIP5P) for Use with Ewald Sums. *J. Chem. Phys.* **2004**, *120*, 6085–6093.

(111) Shirts, M. R.; Klein, C.; Swails, J. M.; Yin, J.; Gilson, M. K.; Mobley, D. L.; Case, D. a.; Zhong, E. D. Lessons learned from comparing molecular dynamics engines on the SAMPL5 dataset. *J. Comput.-Aided Mol. Des.* **2016**, *31*, 147–161.

(112) Rizzi, A.; Jensen, T.; Slochower, D. R.; Aldeghi, M.; Gapsys, V.; Ntekoumes, D.; Bosisio, S.; Papadourakis, M.; Henriksen, N. M.; de Groot, B. L.; Cournia, Z.; Dickson, A.; Michel, J.; Gilson, M. K.; Shirts, M. R.; Mobley, D. L.; Chodera, J. D. The SAMPL6 SAMPLing challenge: assessing the reliability and efficiency of binding free energy calculations. *J. Comput.-Aided Mol. Des.* **2020**, *34*, 601–633.

(113) Rocklin, G. J.; Mobley, D. L.; Dill, K. A.; Hünenberger, P. H. Calculating the binding free energies of charged species based on explicit-solvent simulations employing lattice-

sum methods: An accurate correction scheme for electrostatic finite-size effects. *J. Chem. Phys.* **2013**, *139*, 184103–33.

(114) Kastenholz, M. A.; Hünenberger, P. H. Computation of methodology-independent ionic solvation free energies from molecular simulations. I. The electrostatic potential in molecular liquids. *J. Chem. Phys.* **2006**, *124*, 124106–28.

(115) Kastenholz, M. A.; Hünenberger, P. H. Computation of methodology-independent ionic solvation free energies from molecular simulations. II. The hydration free energy of the sodium cation. *J. Chem. Phys.* **2006**, *124*, 224501–21.

(116) Reif, M. M.; Hünenberger, P. H.; Oostenbrink, C. New Interaction Parameters for Charged Amino Acid Side Chains in the GROMOS Force Field. *J. Chem. Theory Comput.* **2012**, *8*, 3705–3723.

(117) Reif, M. M.; Oostenbrink, C. Net charge changes in the calculation of relative ligand-binding free energies via classical atomistic molecular dynamics simulation. *J. Comput. Chem.* **2013**, *35*, 227–243.

(118) Lin, Y.-L.; Aleksandrov, A.; Simonson, T.; Roux, B. An Overview of Electrostatic Free Energy Computations for Solutions and Proteins. *J. Chem. Theory Comput.* **2014**, *10*, 2690–2709.

Supplementary Information

Supporting Tables

Table S1: Simulated perturbations of TYK2 and the number of particles.

Ligand1	Ligand 2	No. atoms (ligand-only)	No. atoms (protein-ligand)
ejm-44	ejm-55	5954	62290
ejm-49	ejm-31	6521	62288
ejm-31	ejm-46	5888	62281
jmc-28	jmc-27	5886	62282
ejm-42	ejm-48	6014	62290
ejm-31	ejm-43	5950	62286
ejm-50	ejm-42	5630	62272
ejm-42	ejm-55	5633	62275
jmc-23	ejm-46	5884	62277
ejm-31	ejm-45	5638	62283
ejm-55	ejm-54	5729	62278
ejm-45	ejm-42	5639	62284
ejm-31	ejm-48	5960	62284
ejm-47	ejm-31	5906	62290
ejm-47	ejm-55	5915	62290
ejm-44	ejm-42	5956	62295
jmc-23	jmc-27	5886	62276
ejm-43	ejm-55	5951	62281
jmc-23	jmc-30	5884	62277
jmc-28	jmc-30	5887	62286
ejm-42	ejm-54	5640	62282
ejm-49	ejm-50	6517	62290
jmc-23	ejm-55	5887	62289
ejm-31	jmc-28	5889	62291
jmc-23	jmc-27	5886	62276

Table S2: Simulated perturbations of CDK2 and the number of particles.

Ligand1	Ligand 2	No. atoms (ligand-only)	No. atoms (protein-ligand)
22	1h1r	4978	106892
1oiu	26	5885	106905
26	1h1q	5762	106902
17	1h1q	4987	106904
1oiy	1oi9	5675	106908
17	21	4984	106895

Table S3: Calculated $\Delta\Delta G$ values (kcal/mol) and the experimental measured values of simulated perturbations of TYK2. The uncertainty estimates were performed by 1000 bootstrapping trials and are reported as $x_{x_{low}}^{x_{high}}$ where x is the mean value, x_{high} and x_{low} indicate 95% confidence intervals.

Ligand1	Ligand 2	$\Delta\Delta G$ (CPU-PME)	$\Delta\Delta G$ (GPU-PME)	$\Delta\Delta G$ (CPU-RF)	$\Delta\Delta G$ (GPU-RF)	$\Delta\Delta G$ (EXP)
ejm-44	ejm-55	-4.40±0.44	-4.54±0.73	-3.88±0.55	-4.79±0.70	-1.79
ejm-49	ejm-31	-0.89±0.13	-0.57±0.09	-0.81±0.20	-0.59±0.36	-1.79
ejm-31	ejm-46	-0.25±0.21	-0.96±0.17	-0.71±0.07	-0.68±0.11	-1.77
jmc-28	jmc-27	-0.71±0.06	-0.63±0.06	-0.91±0.11	-1.00±0.08	-0.30
ejm-42	ejm-48	0.83±0.23	1.22±0.26	1.01±0.11	1.25±0.24	0.78
ejm-31	ejm-43	1.87±0.11	1.94±0.12	1.58±0.63	1.58±0.41	1.28
ejm-50	ejm-42	-0.24±0.13	0.07±0.12	-0.16±0.11	0.12±0.13	-0.80
ejm-42	ejm-55	-1.17±0.12	-0.95±0.10	-1.05±0.07	-1.07±0.12	0.57
jmc-23	ejm-46	-0.04±0.18	-0.31±0.19	0.13±0.13	0.30±0.13	0.39
ejm-55	ejm-54	-1.10±0.31	-0.86±0.10	-0.99±0.19	-1.22±0.07	-1.32
ejm-45	ejm-42	0.57±0.07	0.12±0.11	0.45±0.12	0.50±0.18	-0.22
ejm-31	ejm-48	0.63±0.34	1.12±0.43	0.94±0.30	0.65±0.72	0.54
ejm-47	ejm-31	-0.12±0.34	-0.27±0.72	-0.30±0.22	-0.20±0.26	0.16
ejm-47	ejm-55	-0.91±0.11	-0.77±0.24	-0.63±0.17	-0.82±0.24	0.49
ejm-44	ejm-42	-2.22±0.11	-2.12±0.36	-2.39±0.64	-1.86±0.27	-2.36
jmc-23	jmc-27	0.07±0.21	0.13±0.16	0.11±0.19	0.28±0.06	0.42
ejm-43	ejm-55	-2.40±0.30	-2.60±0.26	-2.08±0.33	-2.23±0.37	-0.95
jmc-23	jmc-30	-0.38±0.09	-0.29±0.06	-0.22±0.10	-0.06±0.13	0.76
jmc-28	jmc-30	-1.00±0.17	-1.06±0.48	-1.14±0.23	-1.40±0.19	0.04
ejm-42	ejm-54	-1.33±0.17	-1.36±0.18	-1.43±0.11	-1.54±0.12	-0.75
ejm-49	ejm-50	-1.28±0.28	-1.18±0.32	-1.75±0.11	-1.38±0.41	-1.23
jmc-23	ejm-55	0.35±0.33	-0.13±0.17	0.12±0.38	0.09±0.21	2.49
ejm-31	ejm-45	0.47±0.31	0.54±0.22	0.49±0.29	0.61±0.11	-0.02
ejm-31	jmc-28	-0.58±0.24	-0.56±0.17	-0.15±0.41	0.18±0.30	-1.44
RMSE		$1.09_{0.77}^{1.43}$	$1.16_{0.82}^{1.56}$	$1.04_{0.76}^{1.35}$	$1.20_{0.83}^{1.61}$	
MUE		$0.86_{0.61}^{1.14}$	$0.93_{0.66}^{1.27}$	$0.86_{0.64}^{1.10}$	$0.94_{0.66}^{1.27}$	

Table S4: Simulation wallclock time (min) of TYK2.

Simulation	complex	ligand-only
CPU-PME	2838.2±328.1	288.1±27.6
GPU-PME	185.4±4.12	69.0±3.8
CPU-RF	1903.7±334.2	211.6±20.5
GPU-RF	204.7±5.9	66.0±4.8

Table S5: Simulation wallclock time (min) of CDK2.

Simulation	complex	ligand-only
CPU-PME	4447.3±423.7	252.8±24.7
GPU-PME	326.8±6.5	83.1±3.8
CPU-RF	3143.0±204.5	210.2±21.9
GPU-RF	325.9±11.9	77.2±4.3